Two-dimensional *R*-matrix propagator: Application to electron-hydrogen scattering

K. M. Dunseath, M. Le Dourneuf, M. Terao-Dunseath, and J.-M. Launay
Laboratoire de Simulation des Interatctions entre Molécules, Photons et Atomes, EP 99 du CNRS, Bâtiment 22, Campus de Beaulieu, Université de Rennes I, 35042 Rennes Cedex, France
(Received 12 February 1996)

The two-dimensional *R*-matrix propagator of Le Dourneuf *et al.* [J. Phys. B **23**, L559 (1990)] is generalized to arbitrary angular momenta and applied to the study of electron-hydrogen collisions at energies up to the $n=5$ threshold. Results are presented for phase shifts, resonance positions and widths, as well as cross sections for partial waves of total angular momenta $L\leqslant 3$. The stability and efficiency of the method are established. A comparison is made below the $n=3$ threshold with results from other theories. Agreement is very good, in particular with the results of a finite-difference numerical integration of the Schrödinger equation by Wang and Callaway [Phys. Rev. A **50**, 2327 (1994)]. Partial cross sections for ^1S between the $n=3$ and 5 thresholds illustrate the potential of the method for studying excitation into high Rydberg states. [S1050-2947(96)05107-4]

PACS number(s): 34.80.Bm, 31.15.Ar, 34.80.Dp

I. INTRODUCTION

Electron-hydrogen scattering possesses several features that make it a severe test for theoretical descriptions of electronic collisions. Since the charge on the nucleus is small, correlation effects between the bound and scattered electrons are particularly important. The scattering is strongly influenced by long-range multipole couplings, notably by the dynamical polarizability, induced by virtual transitions to closed channels including the continuum [1,2], and by the dipole coupling between degenerate states which gives rise to infinite series of resonances converging to the excitation thresholds [3].

After more than 30 years of study there exists a wealth of theoretical and experimental data with which any new theory can be compared (see, for example, [4], and references therein). Much work has been done using the close-coupling approximation and variants [5–11]. The main feature of these methods is the expansion of the wave function for the electron-atom system over a discrete set including target stationary states and pseudostates which are essential to obtain accurate cross sections. Recent efforts have thus been devoted to defining new bases with faster convergence properties [11,12].

The simplicity of the two-electron Schrödinger equation has also encouraged the development of approaches based on direct numerical integration rather than basis expansions. Early work by Temkin [13], Poet [14], and Callaway and Oza [15] considered a model restricted to *s* waves, the results of which remain a benchmark for new methods [12,16,17]. Recently, two direct numerical integration methods have been developed for the full scattering problem: a finite-element method [18] and a finite-difference propagation method [19]. These two approaches, based on very different numerical algorithms, give similar results.

The close-coupling approach has also been extended to include the double continuum of the collisional system. This approach has been implemented within the framework of *R*-matrix theory by Burke and co-workers [20–22], with the configuration space of the two electrons divided into an inner and an outer region. A further extension is to subdivide the two-dimensional (2D) configuration space into elementary domains where a locally adapted expansion is used. Le Dourneuf *et al.* [16] proposed a method to propagate the *R* matrix from the origin throughout these domains to a distance where an asymptotic solution may be defined. This was implemented and tested on the *s*-wave model of *e*-H scattering. The results obtained are in excellent agreement with those of Temkin [13], Poet [14], and Callaway and Oza [15]. They establish the numerical stability and efficiency of the method for the electron-impact excitation of Rydberg states, together with the possibility of treating ionization.

In this paper we generalize the 2D *R*-matrix propagation method to arbitrary angular momenta, and apply it to the full electron-hydrogen scattering problem. The outline of the paper is as follows. In Sec. II we present in detail the theory of propagating the *R* matrix in two dimensions. In Sec. III we apply the method to *e*-H scattering. We make a detailed comparison of our results with previous calculations up to the $n=3$ excitation threshold and give partial cross sections for ^1S up to the $n=5$ threshold. We use atomic units except where otherwise stated.

II. THEORY

We consider an atomic system consisting of a nucleus of charge Z and two electrons. We write the wave function Φ for the two-electron system as

$$\Phi(\boldsymbol{r}_1,\boldsymbol{r}_2)=\frac{1}{r_1 r_2}\Psi(\boldsymbol{r}_1,\boldsymbol{r}_2). \tag{2.1}$$

The Schrödinger equation satisfied by the wave function $\Psi(\boldsymbol{r}_1,\boldsymbol{r}_2)$ at energy E is

$$(H-E)\Psi=0, \tag{2.2}$$

where the Hamiltonian H is given by

$$H=h_1+h_2+\frac{1}{r_{12}}, \tag{2.3}$$

with

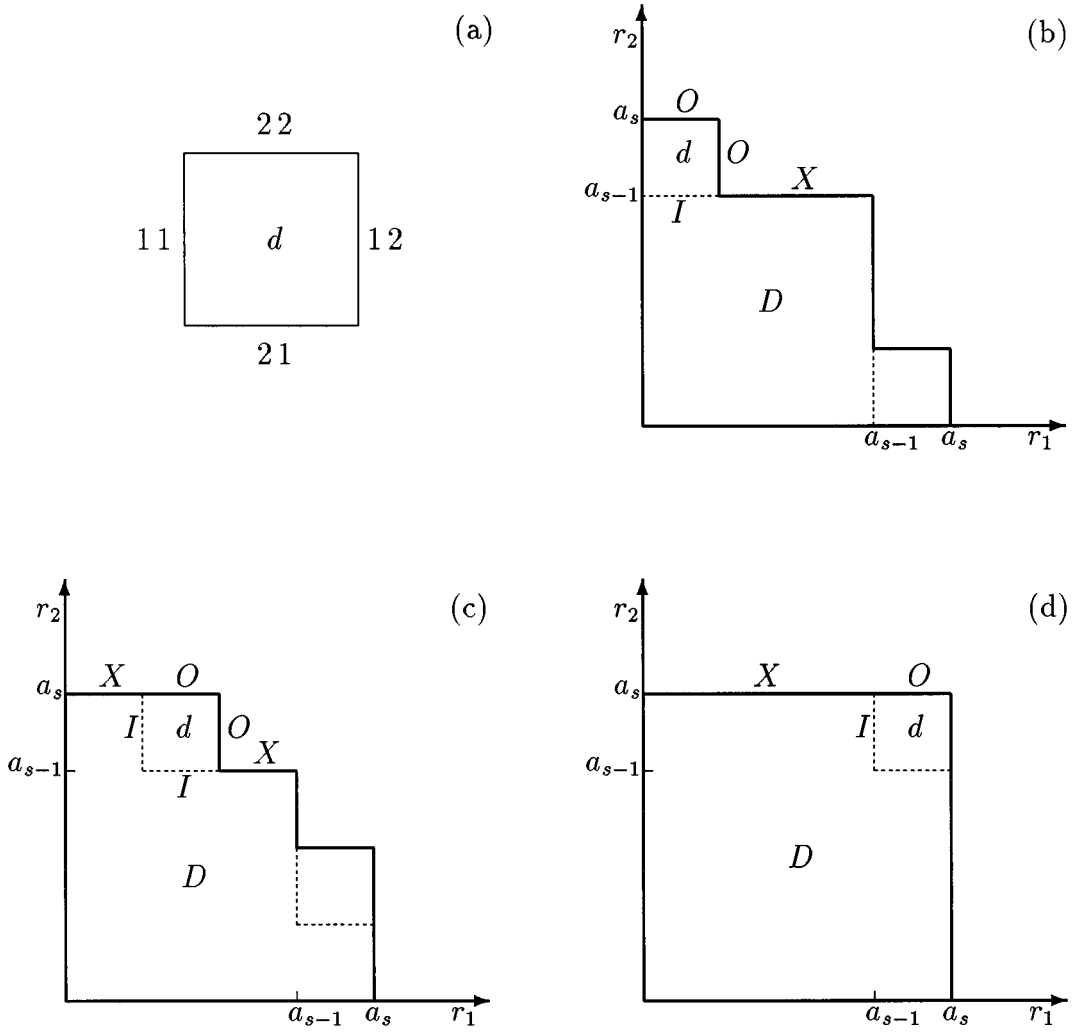

FIG. 1. Subdivision of the two-dimensional configuration space into elementary domains and the labeling scheme for each side of a typical domain. In (a) the four boundaries of a typical domain d are labeled by the pair of indices cb, where $c=1,2$ labels the electron with fixed radial coordinate and $b=1,2$ specifies the lower and upper boundaries. In (b) the domain d is being added to the domain D, boundary $X+I$, to give a domain D', boundary $X+O$. By symmetry, we need only consider half of the (r_1-r_2) plane; we choose to work in the upper half. The input border I consists of only one side ($cb=21$) as the r matrix is zero when $r_1=0$ ($cb=11$). In (c) the domain d does not lie on an edge or on the diagonal; in this case the input and output borders I and O consist of two sides 11, 21 and 12, 22, respectively. In (d) the domain d lies on the diagonal; by symmetry we need only consider one side of the input and output borders, providing that we multiply the elements of the corresponding r matrix by 2.

$$h_c=-\frac{1}{2}\frac{d^2}{dr_c^2}+\frac{l_c^2}{2r_c^2}-\frac{Z}{r_c}\quad(c=1,2),\tag{2.4}$$

l_c denoting the one-electron orbital angular momentum operator.

The key idea of the method is to partition the two-electron configuration space into elementary domains (see Fig. 1). Since the problem is symmetric in $\boldsymbol{r}_1$ and $\boldsymbol{r}_2$, we divide the range of each radial coordinate in the same way, in sectors $s=[a_{s-1},a_s]$. A domain $s_1\times s_2$ is defined by the set of radial coordinates $\{r_1\in[a_{s_1-1},a_{s_1}],\ r_2\in[a_{s_2-1},a_{s_2}]\}$. In each sector, we define a basis of orbitals which we then use to construct bases of two-electron functions in each domain.

A. One-electron basis

In sector $s=[a_{s-1},a_s]$ we define the orbitals $u_{nl}(r)$ with angular momentum l as solutions of the eigenvalue problem

$$(\tilde{h}-\epsilon_{nl})u_{nl}(r)=0,\tag{2.5}$$

where the one-electron modified Hamiltonian is given by

$$\tilde{h}=-\frac{1}{2}\left[\frac{d^2}{dr^2}+\delta(r-a_{s-1})\frac{d}{dr}-\delta(r-a_s)\frac{d}{dr}\right]-\frac{Z}{r}+\frac{l(l+1)}{2r^2}.\tag{2.6}$$

The Bloch operators [23] at the two end points ensure the hermiticity of $\tilde{h}$ in the sector.

To solve (2.5) we expand $u_{nl}(r)$ in a basis of N_P Legendre polynomials $P_n(x)$, with $x=(2r-a_s-a_{s-1})/(a_s-a_{s-1})$. The expansion coefficients are obtained by diagonalizing the operator $\tilde{h}$ in this basis. We note that the volume element of the integrals occurring in the matrix rep-

resentation of $\tilde{h}$ is simply $dr\ d\Omega$, since we are working with the wave function Ψ defined by (2.1). In the first sector ($s=1$), which contains the origin, we diagonalize $\tilde{h}$ (without a Bloch operator at $a_0=0$) in the nonorthogonal basis $rP_n(x)$ where the additional factor r ensures that eigenfunctions regular at the origin are selected.

The orbitals $u_{nl}(r)$ and the associated eigenvalues ϵ_{nl} depend on the sector. To avoid cumbersome notation, the sector index will not be specified, except when necessary.

B. Two-electron basis

In a fixed domain $s_1\times s_2=[a_{s_1-1},\ a_{s_1}]\times[a_{s_2-1},\ a_{s_2}]$, it is convenient to label the four boundaries by the pair of indices cb, where $c=1,2$ labels the electron with fixed radial coordinate and $b=1,2$ specifies the lower and upper boundaries [see Fig. 1(a)]. The value of coordinate r_c at boundary b is denoted by a_{cb}. For given total orbital momentum L, spin S, and parity π, a discrete R-matrix basis is obtained by solving the eigenvalue problem

$$(H+L_B-E_k)\Psi_k=0, \tag{2.7}$$

where Hermiticity in the domain is ensured by inclusion of the Bloch operator

$$L_B=\frac{1}{2}\sum_{c=1}^{2}\sum_{b=1}^{2}(-1)^b\delta(r_c-a_{cb})\frac{\partial}{\partial r_c}. \tag{2.8}$$

In diagonal domains, the eigenfunctions Ψ_k are expanded for each spin as

$$\Psi_k=\sum_{\substack{n_1l_1\\ n_2l_2}}\alpha_{n_1l_1n_2l_2k}\,\mathcal{A}\,u_{n_1l_1}(r_1)u_{n_2l_2}(r_2)\mathcal{Y}^{LM_L}_{l_1l_2}, \tag{2.9}$$

where $\mathcal{A}=\mathcal{N}[1+(-1)^SP_{12}]$ is the (anti)symmetrization operator, P_{12} the permutation operator, and $\mathcal{N}=1/\sqrt{2}$, except for $(n_1,l_1)=(n_2,l_2)$ where $\mathcal{N}=1/2$. The angular factor is

$$\mathcal{Y}^{LM_L}_{l_1l_2}=\sum_{m_1m_2}(l_1m_1l_2m_2|LM_L)Y_{l_1m_1}(\hat{\mathbf{r}}_1)Y_{l_2m_2}(\hat{\mathbf{r}}_2),$$

where $(l_1m_1l_2m_2|LM_L)$ are Clebsch-Gordan coefficients [24] and $Y_{lm}(\hat{\mathbf{r}})$ are spherical harmonics.

In off-diagonal domains, where the two coordinates r_1 and r_2 span different subspaces, there is no exchange contribution to the matrix elements. The eigenvalue problem is therefore independent of the total spin S, and is solved once using the unsymmetrized expansion

$$\Psi_k=\sum_{\substack{n_1l_1\\ n_2l_2}}\alpha_{n_1l_1n_2l_2k}u_{n_1l_1}(r_1)u_{n_2l_2}(r_2)\mathcal{Y}^{LM_L}_{l_1l_2}. \tag{2.10}$$

In expansions (2.9) and (2.10), the two-electron basis is built from the first N_O solutions of (2.5) for each orbital momentum l_c. The remaining N_P-N_O orbitals are included in the Buttle correction which accounts approximately for the terms omitted in the two-electron basis (see below).

C. R-matrix relations in an elementary domain

The Schrödinger equation (2.2), rewritten as

$$(H+L_B-E)|\Psi\rangle=L_B|\Psi\rangle, \tag{2.11}$$

is solved using the spectral representation of $(H+L_B-E)^{-1}$:

$$|\Psi\rangle=\sum_k|\Psi_k\rangle\frac{1}{E_k-E}\langle\Psi_k|L_B\Psi\rangle. \tag{2.12}$$

The R-matrix relations are obtained by projecting (2.12) onto the channel functions

$$\phi_i^{\ell}(r_{\ell},\ \hat{\mathbf{r}}_1,\ \hat{\mathbf{r}}_2)=u_{n_{\ell}l_{\ell}}(r_{\ell})\mathcal{Y}^{LM_L}_{l_1l_2}, \tag{2.13}$$

with the collective channel index $i=\{n_{\ell}l_{\ell}l_c\}$ and $\ell=2,1$ when $c=1,2$, respectively. By evaluating these projections on the four boundaries $r_c=a_{cb}$, we obtain a set of linear equations

$$f_i^{(cb)}=\sum_{c'=1}^{2}\sum_{b'=1}^{2}\sum_{i'}(-1)^{b'}r_{ii'}^{(cb,c'b')}d_{i'}^{(c'b')} \tag{2.14}$$

between the amplitudes of the radial functions

$$f_i^{(cb)}=\langle\phi_i^{(\ell)}|\,\delta(r_c-a_{cb})\Psi\rangle \tag{2.15}$$

and their derivatives

$$d_i^{(cb)}=\left\langle\phi_i^{(\ell)}\middle|\,\delta(r_c-a_{cb})\frac{\partial}{\partial r_c}\Psi\right\rangle \tag{2.16}$$

in terms of the elementary r matrix

$$r_{ii'}^{(cb,c'b')}=\frac{1}{2}\sum_k\frac{\Gamma_{ik}^{(cb)}\Gamma_{i'k}^{(c'b')}}{E_k-E}, \tag{2.17}$$

which depends on the energies E_k of the eigenstates Ψ_k and their surface amplitudes

$$\Gamma_{ik}^{(cb)}=\langle\phi_i^{(\ell)}|\,\delta(r_c-a_{cb})|\Psi_k\rangle=\sum_{n_c=1}^{N_O}\alpha_{n_1l_1n_2l_2k}u_{n_cl_c}(a_{cb}). \tag{2.18}$$

In (2.17), the summation over k is limited by the size of the two-electron basis. The effect of this truncation is significant even when the number of terms retained is large. It is approximately accounted for by a Buttle correction [25], based on the solution of an approximate problem in which all channel couplings are neglected. The resulting r matrix is then diagonal. In our case, the correction in channel $i=\{n_{\ell}l_{\ell}l_c\}$ is given by the remainder of this r matrix:

$$\tilde{r}_{ii'}^{(cb,c'b')}=\frac{1}{2}\delta_{ii'}\delta_{cc'}\sum_{k=N_O+1}^{N_P}\frac{u_{kl_c}^{(s_c)}(a_{cb})u_{kl_c}^{(s_c)}(a_{cb'})}{\epsilon_{n_\ell l_\ell}^{(s_\ell)}+\epsilon_{kl_c}^{(s_c)}-E}, \tag{2.19}$$

where $\epsilon_{n_\ell l_\ell}^{(s_\ell)}$ and $\epsilon_{kl_c}^{(s_c)}$ are the eigenenergies of the orbitals $u_{n_\ell l_\ell}^{(s_\ell)}$ and $u_{kl_c}^{(s_c)}$. In practice, the series in (2.19) converges quickly because the Legendre functions have nonzero derivatives on the boundaries [26].

Denoting the input sides $\{cb=11,21\}$ by I and the output sides $\{cb=12,22\}$ by O, we may write (2.14) in block matrix notation

$$\begin{pmatrix}\boldsymbol{f}_I\\ \boldsymbol{f}_O\end{pmatrix}=\begin{pmatrix}-\boldsymbol{r}_{II} & \boldsymbol{r}_{IO}\\ -\boldsymbol{r}_{OI} & \boldsymbol{r}_{OO}\end{pmatrix}\begin{pmatrix}\boldsymbol{d}_I\\ \boldsymbol{d}_O\end{pmatrix}. \tag{2.20}$$

D. *R*-matrix propagation

Relations of the form (2.20) are valid for any shape and size of the 2D domain. The radial functions and derivatives on the boundary $X+I$ of a global domain D can therefore be related to those on the boundary $X+O$ of an extended domain $D'=D+d$ by

$$\begin{pmatrix}\boldsymbol{f}_X\\ \boldsymbol{f}_I\end{pmatrix}=\begin{pmatrix}-\boldsymbol{R}_{XX}^{D} & \boldsymbol{R}_{XI}^{D}\\ -\boldsymbol{R}_{IX}^{D} & \boldsymbol{R}_{II}^{D}\end{pmatrix}\begin{pmatrix}\boldsymbol{d}_X\\ \boldsymbol{d}_I\end{pmatrix}, \tag{2.21a}$$

$$\begin{pmatrix}\boldsymbol{f}_X\\ \boldsymbol{f}_O\end{pmatrix}=\begin{pmatrix}-\boldsymbol{R}_{XX}^{D'} & \boldsymbol{R}_{XO}^{D'}\\ -\boldsymbol{R}_{OX}^{D'} & \boldsymbol{R}_{OO}^{D'}\end{pmatrix}\begin{pmatrix}\boldsymbol{d}_X\\ \boldsymbol{d}_O\end{pmatrix}. \tag{2.21b}$$

The elimination of $\boldsymbol{f}_I$ and $\boldsymbol{d}_I$ between Eqs. (2.20) and (2.21a) gives the R-matrix propagation relations [16]

$$\begin{aligned}
\boldsymbol{R}_{OO}^{D'}&=\boldsymbol{r}_{OO}-\boldsymbol{r}_{OI}(\boldsymbol{r}_{II}+\boldsymbol{R}_{II}^{D})^{-1}\boldsymbol{r}_{IO},\\
\boldsymbol{R}_{OX}^{D'}&=\boldsymbol{r}_{OI}(\boldsymbol{r}_{II}+\boldsymbol{R}_{II}^{D})^{-1}\boldsymbol{R}_{IX}^{D},\\
\boldsymbol{R}_{XO}^{D'}&=\boldsymbol{R}_{XI}^{D}(\boldsymbol{r}_{II}+\boldsymbol{R}_{II}^{D})^{-1}\boldsymbol{r}_{IO},\\
\boldsymbol{R}_{XX}^{D'}&=\boldsymbol{R}_{XX}^{D}-\boldsymbol{R}_{XI}^{D}(\boldsymbol{r}_{II}+\boldsymbol{R}_{II}^{D})^{-1}\boldsymbol{R}_{IX}^{D}.
\end{aligned} \tag{2.22}$$

The relations (2.22) allow the R matrix to be propagated out from the origin to some distance $r_1=r_2=r_{\text{out}}$. Since the problem is symmetric in the coordinates $\boldsymbol{r}_1,\boldsymbol{r}_2$, the R matrices are symmetric and need only be propagated in a half plane.

There are obviously different strategies for assembling the elementary domains. The one we have adopted is illustrated in Fig. 1. In the upper half of the configuration space, we consider successive horizontal strips $\mathcal{S}=[0,a_s]\times[a_{s-1},a_s]$. We fill each strip by assembling elementary domains with increasing r_1, starting at the left [Fig. 1(b)] and ending at the diagonal [Fig. 1(d)] through s applications of (2.22) [Fig. 1(c)]. For most domains, both the input border I and the output border O consists of the two sides, $\{cb=11,21\}$ and $\{cb=12,22\}$, respectively. However, for the first domain of each strip, I has only one side (regular functions being zero on $\{cb=11\}$) while O has two sides, hence the global dimension of the R matrix increases as it is assembled. In the diagonal domain, symmetry imposes that the elementary r matrix is identical on both input sides I or both output sides O, so we can consider that I and O have only one side, provided the corresponding r-matrix elements (2.17) are multiplied by 2.

E. Matching to asymptotic solutions

The 2D R matrix is propagated out to the the boundary of a global square domain D_{out} defined by $r_1,r_2\leqslant r_{\text{out}}$, where the exchange between the two electrons becomes negligible for the process of interest. For low-energy electron-impact excitation of Rydberg states, this condition is always satisfied for sufficiently large r_{out}. The distant interaction between the target and the escaping electron can thus be described by a 1D propagation using the close-coupling formalism:

$$\Psi_j(\boldsymbol{r}_1,\boldsymbol{r}_2)=\sum_i \phi_i(\boldsymbol{r}_1,\hat{\boldsymbol{r}}_2)F_{ij}(r_2), \tag{2.23}$$

where $F_{ij}(r_2)$ are the unknown radial functions for the free electron. The channel functions ϕ_i are formed by coupling the angular function of the free electron with *R-matrix eigenstates of the target electron*, which diagonalize the one-electron operator (2.6) in the *global* sector $[0,r_{\text{out}}]$. This diagonalization yields a discrete set of basis functions $v_{nl}(r_1)$, of which the lowest correspond very precisely to the first hydrogenic bound states. The size of the global basis used to diagonalize (2.6) depends on r_{out}, while the number of orbital functions v_{nl} retained depends on the collision energy. We have found that it is generally sufficient to retain orbitals whose energies are up to 1.5 times the collision energy. At very low collision energies, a minimum number of states has to be retained.

At the boundary r_{out}, the R matrix $\mathcal{R}$ in the close-coupling basis (2.23) is obtained from the R matrix $\boldsymbol{R}$ in the 2D propagation basis by a unitary transformation

$$\mathcal{R}=\boldsymbol{U}^T\boldsymbol{R}\boldsymbol{U}. \tag{2.24}$$

The elements of the matrix $\boldsymbol{U}$ are the projections of the one-electron R-matrix states in each sector $s=[a_{s-1},a_s]$, onto those in the global sector $[0,r_{\text{out}}]$,

$$U_{snl,n'l}=\langle u_{nl}^{(s)}|v_{n'l}\rangle=\int_{a_{s-1}}^{a_s}u_{nl}^{(s)}(r)v_{n'l}(r)dr. \tag{2.25}$$

Substituting the expansion (2.23) into the Schrödinger equation leads to a set of coupled second-order differential equations for the unknown functions F_{ij}, which can be solved using the methods described by Burke and Noble [27]. If necessary, the R matrix $\mathcal{R}$ is first propagated in 1D using a method developed by Light and Walker [28], out to a distance r_{asy} where it is matched to a set of independent asymptotic solutions propagated inwards by an analytic expansion method [29,30]. This provides N_{open} independent physical solutions j with asymptotic form

TABLE I. Comparison of phase shifts for e-H scattering: RM2D(N_O), 2D R-matrix propagator with N_O orbitals for each angular momentum; FDPM, finite-difference numerical integration of the 2D Schrödinger equation [19]; FEM, finite-element method [18]; IERM, intermediate-energy R matrix method [21]; var, variational methods (S [32]; P^o [33]; D [34]; F^o [35]).

	k	0.1	0.2	0.3	0.4	0.5	0.6	0.7	0.8
^1S	RM2D(15)	2.553	2.066	1.695	1.414	1.200	1.039	0.929	0.886
	RM2D(20)	2.553	2.066	1.696	1.414	1.200	1.040	0.930	0.886
	FDPM	2.555	2.066	1.695	1.415	1.200	1.041	0.930	0.887
	FEM	2.553	2.066	1.695	1.414	1.200	1.040	0.930	0.887
	IERM	2.550	2.062	1.691	1.410	1.196	1.035	0.925	
	var	2.556	2.067	1.696	1.415	1.201	1.041	0.930	0.887
^3S	RM2D(15)	2.939	2.718	2.500	2.294	2.105	1.933	1.780	1.645
	RM2D(20)	2.939	2.718	2.500	2.294	2.105	1.933	1.780	1.644
	FDPM	2.939	2.717	2.500	2.294	2.104	1.933	1.780	1.644
	FEM	2.938	2.717	2.500	2.294	2.104	1.933	1.780	1.645
	IERM	2.939	2.717	2.500	2.294	2.105	1.933	1.780	
	var	2.939	2.717	2.500	2.294	2.105	1.933	1.779	1.644
$^1P^o$	RM2D(15)	0.006	0.015	0.016	0.009	−0.002	−0.012	−0.015	−0.007
	RM2D(20)	0.006	0.015	0.016	0.009	−0.002	−0.012	−0.015	−0.007
	FDPM	0.006	0.016	0.017	0.010	−0.002	−0.012	−0.015	−0.007
	FEM	0.006	0.015	0.016	0.009	−0.002	−0.012	−0.015	−0.007
	IERM	0.006	0.015	0.016	0.009	−0.002	−0.012	−0.016	
	var	0.006	0.015	0.017	0.010	−0.001	−0.011	−0.014	−0.006
$^3P^o$	RM2D(15)	0.010	0.045	0.107	0.187	0.270	0.341	0.393	0.428
	RM2D(20)	0.010	0.045	0.107	0.187	0.270	0.341	0.393	0.427
	FDPM	0.010	0.046	0.107	0.188	0.271	0.342	0.394	0.429
	FEM	0.010	0.045	0.107	0.187	0.271	0.342	0.393	0.428
	IERM	0.010	0.045	0.107	0.187	0.270	0.341	0.392	
	var	0.010	0.045	0.107	0.187	0.271	0.341	0.393	0.427
^1D	RM2D(15)	0.0013	0.0052	0.011	0.019	0.028	0.039	0.052	0.075
	FDPM	0.0012	0.0056	0.011	0.018	0.027	0.038	0.052	0.075
	FEM	0.0007	0.0048	0.011	0.018	0.027	0.038	0.052	0.074
	IERM	0.0013	0.0051	0.011	0.018	0.027	0.038	0.052	
	var	0.0012	0.0052	0.011	0.018	0.027	0.038	0.052	0.075
^3D	RM2D(15)	0.0013	0.0053	0.012	0.020	0.031	0.043	0.056	0.070
	FDPM	0.0012	0.0057	0.011	0.020	0.030	0.042	0.055	0.070
	FEM	0.0007	0.0049	0.011	0.020	0.030	0.042	0.055	0.070
	IERM	0.0013	0.0052	0.011	0.020	0.030	0.042	0.055	
	var	0.0013	0.0052	0.011	0.020	0.030	0.042	0.055	0.070
$^1F^o$	RM2D(15)	0.0004	0.0018	0.0040	0.0069	0.011	0.015	0.021	0.026
	FDPM	0.0001	0.0015	0.0038	0.0064	0.010	0.015	0.020	0.026
	FEM	0.0000	0.0016	0.0037	0.0065	0.010	0.015	0.020	0.026
	var			0.0038	0.0066	0.010	0.015	0.020	0.026
$^3F^o$	RM2D(15)	0.0004	0.0018	0.0040	0.0069	0.011	0.015	0.021	0.027
	FDPM	0.0001	0.0015	0.0038	0.0064	0.010	0.015	0.020	0.026
	FEM	0.0000	0.0016	0.0037	0.0065	0.010	0.015	0.020	0.026
	var			0.0038	0.0067	0.010	0.015	0.020	0.026

$$F_{ij}(r) \underset{r\to\infty}{\sim} k_i^{-1/2}(\sin\theta_i\delta_{ij}+\cos\theta_i K_{ij}),$$
$$F_{ij}(r) \underset{r\to\infty}{\sim} 0, \tag{2.26}$$

respectively, for open and closed channels i. The K_{ij} are elements of the standard K matrix, $\theta_i = k_i r - 1/2 l_i \pi$ for neutral targets, $k_i^2/2 = (E - E_i)$ is the channel energy, and E_i the energy of the target state in channel i. The S matrix is obtained from the K matrix by the relation

$$\boldsymbol{S} = \frac{\mathbf{1}+i\boldsymbol{K}}{\mathbf{1}-i\boldsymbol{K}}. \tag{2.27}$$

The $LS\pi$ partial cross section for the transition from an initial target state $n_1 l_1$ to a final target state $n_1' l_1'$ is given by

TABLE II. Positions and widths of the lowest ^1S, $^3P^o$, and ^1D resonances below the $n=2$ threshold. Present results (RM2D) are compared with those of the finite-difference propagation method (FDPM) [19], the finite-element method (FEM) [18], the IERM method [21], a hyperspherical coordinate calculation (HC) [36], and experimental results [37–39].

State	Method	Position (eV)	Width (eV)
^1S	RM2D	9.557	0.0473
	FDPM	9.557	0.0472
	FEM	9.559	0.0472
	IERM	9.557	0.0471
	HC	9.559	0.0475
	expt [37]	9.558	
	expt [38]	9.557	0.045
	expt [39]	9.549	0.063
$^3P^o$	RM2D	9.738	0.0058
	FDPM	9.739	0.0058
	FEM	9.738	0.0058
	IERM	9.738	0.0057
	HC	9.745	0.0077
	expt [37]	9.738	0.0056
	expt [38]	9.735	0.006
	expt [39]	9.738	0.0057
^1D	RM2D	10.125	0.0087
	FDPM	10.125	0.0091
	FEM	10.128	0.0093
	IERM	10.125	0.0088
	HC	10.129	0.0101
	expt [39]	10.115	0.006

$$\sigma^{LS\pi}_{n_1 l_1 \to n_1' l_1'} = \frac{\pi}{4k_i^2} \frac{(2L+1)(2S+1)}{(2l_1+1)} \sum_{l_2 l_2'} |S_{ii'} - \delta_{ii'}|^2,$$

where $i=\{n_1 l_1 l_2\}$ and $i'=\{n_1' l_1' l_2'\}$. The total cross section is obtained by summing all $LS\pi$ contributions. The sum over L, infinite in principle, is truncated in practice at some value $L_{\max}$ chosen large enough to ensure convergence.

III. RESULTS AND DISCUSSION

To test the 2D R-matrix propagation method for the full e-H scattering problem, we have calculated phase shifts, resonance parameters and partial cross sections below the $n=3$ threshold. We make a very detailed comparison with the recent numerical results of Wang and Callaway [19], who used a finite-difference propagation method (FDPM) of Numerov type (extending that used by Poet [14]), together with a Burke-Schey asymptotic expansion [29]. Wherever possible we have chosen the parameters in our calculation to match those used by Wang and Callaway. We have in particular included the same angular couplings: for $L=0$, $(l_1 l_2)=(00),(11),(22),(33)$; for $L=1$, $(l_1 l_2)=(10),(01),(21),(12),(32),(23)$; for $L=2$, $(l_1 l_2)=(20),(02),(31),(13),(11),(22)$; for $L=3$, $(l_1 l_2)=(30),(03),(12),(21),(14),(41)$.

We have performed the 2D propagation in steps of 10 a.u. out to 60 a.u., beyond which we have used the 1D Light-Walker propagator and a Gailitis asymptotic expansion [30]. We have established the convergence of our results with the distance of 2D propagation, by comparing the cross sections obtained for $r_{\text{out}}=40$, 50, and 60 a.u. At 40 a.u., we obtain a good representation of the $n=3$ states of hydrogen, while at 60 a.u. the $n=4$ energies become accurate to 10^{-5} Ry. The cross sections for all possible transitions differ by at most

TABLE III. Cross sections (in units of πa_0^2) for transitions between the $n=1$ and 2 states at a collision energy of 0.76 Ry. The present results are compared with those of the finite-difference propagation method (FDPM) [19].

	Method	^1S	^3S	$^1P^o$	$^3P^o$	^1D	^3D	$^1F^o$	$^3F^o$
$1s$-$1s$:	RM2D(15)	0.661	3.945	0.0014	2.110	0.051	0.128	0.010	0.031
	RM2D(20)	0.662	3.945	0.0014	2.111				
	FDPM	0.661	3.945	0.0014	2.123	0.051	0.129	0.010	0.032
$1s$-$2s$:	RM2D(15)	0.037	0.0005	0.0079	0.036	0.053	0.000009	0.00004	0.0003
	RM2D(20)	0.037	0.0005	0.0079	0.036				
	FDPM	0.037	0.0005	0.0078	0.036	0.053	0.000003	0.00004	0.0003
$1s$-$2p$:	RM2D(15)	0.028	0.0004	0.065	0.037	0.091	0.0002	0.0001	0.0010
	RM2D(20)	0.028	0.0004	0.065	0.037				
	FDPM	0.028	0.0004	0.065	0.037	0.090	0.0002	0.0001	0.0009
$2s$-$2s$:	RM2D(15)	8.052	121.5	48.42	317.2	144.2	73.03	57.62	162.4
	RM2D(20)	8.058	121.5	48.40	317.3				
	FDPM	8.079	121.6	48.44	317.1	143.9	72.46	57.71	162.6
$2s$-$2p$:	RM2D(15)	15.67	68.84	61.76	195.4	114.0	236.0	142.9	420.7
	RM2D(20)	15.67	68.86	61.75	195.5				
	FDPM	15.67	68.84	61.71	195.4	113.9	235.5	142.9	420.4
$2p$-$2p$:	RM2D(15)	19.68	29.65	87.47	329.3	110.8	638.0	158.0	493.5
	RM2D(20)	19.68	29.65	87.51	329.3				
	FDPM	19.67	29.64	87.43	329.7	110.9	638.1	157.9	493.0

TABLE IV. As for Table III, but at a collision energy of 0.78 Ry.

	Method	^1S	^3S	$^1P^o$	$^3P^o$	^1D	^3D	$^1F^o$	$^3F^o$
$1s$-$1s$:	RM2D(15)	0.623	3.841	0.001	2.064	0.058	0.131	0.010	0.033
	RM2D(20)	0.624	3.841	0.001	2.064				
	FDPM	0.622	3.841	0.001	2.073	0.058	0.131	0.010	0.033
$1s$-$2s$:	RM2D(15)	0.041	0.001	0.0032	0.044	0.055	0.0005	0.0003	0.0034
	RM2D(20)	0.041	0.001	0.0032	0.044				
	FDPM	0.041	0.001	0.0032	0.044	0.056	0.0004	0.0003	0.0035
$1s$-$2p$:	RM2D(15)	0.035	0.0004	0.048	0.041	0.092	0.0015	0.001	0.010
	RM2D(20)	0.035	0.0004	0.048	0.041				
	FDPM	0.035	0.0004	0.048	0.042	0.092	0.0017	0.001	0.011
$2s$-$2s$:	RM2D(15)	5.314	0.570	51.54	66.50	64.29	81.41	19.53	37.34
	RM2D(20)	5.312	0.565	51.53	66.49				
	FDPM	5.313	0.570	51.47	66.18	64.15	81.39	19.56	37.36
$2s$-$2p$:	RM2D(15)	0.962	6.867	18.02	7.209	17.30	118.97	47.85	120.9
	RM2D(20)	0.962	6.831	18.01	7.225				
	FDPM	0.960	6.854	18.00	7.218	17.29	118.94	47.81	120.8
$2p$-$2p$:	RM2D(15)	9.316	27.98	11.29	164.1	55.41	139.5	49.34	192.3
	RM2D(20)	9.317	28.01	11.30	164.0				
	FDPM	9.334	27.98	11.33	164.2	55.49	139.4	49.29	192.1

one in the last figure given, with those for the triplet converging much faster than for the singlet. The cross sections are more sensitive to the number of orbitals N_O used in the expansion of the two-electron wave function. To illustrate this convergence, we present results for $N_O=15$ [denoted by RM2D(15)], and $N_O=20$ [denoted by RM2D(20)]. The results agree in general to within 1%.

We have also included where possible the results of other accurate calculations, in particular those of the finite-element method (FEM) [18], the convergent close-coupling method (CCC) [11,31] and the intermediate-energy R-matrix method (IERM) [21]. The FEM calculation does not take into account the long-range asymptotic couplings explicitly, avoiding these by solving the problem in a 2D region sufficiently large for the scattering energy under consideration (64 a.u. at 0.81 Ry). In the CCC method, a basis of Laguerre polynomials is used and the close-coupling equations are solved in momentum space [11]. Convergence is tested by increasing the basis size. The IERM method uses a two-electron basis expansion similar to (2.9), but defined in a single large box of 25 a.u. and built with numerical orbitals which are solutions of a second-order differential equation with fixed logarithmic boundary conditions rather than an expansion in shifted Legendre polynomials.

TABLE V. As for Table III, but at a collision energy of 0.80 Ry.

	Method	^1S	^3S	$^1P^o$	$^3P^o$	^1D	^3D	$^1F^o$	$^3F^o$
$1s$-$1s$:	RM2D(15)	0.587	3.741	0.0013	2.016	0.062	0.133	0.011	0.034
	RM2D(20)	0.588	3.741	0.0013	2.016				
	FDPM	0.586	3.742	0.0013	2.024	0.062	0.133	0.011	0.034
$1s$-$2s$:	RM2D(15)	0.053	0.001	0.0031	0.049	0.059	0.0019	0.0006	0.0080
	RM2D(20)	0.053	0.001	0.0031	0.050				
	FDPM	0.053	0.001	0.0031	0.050	0.058	0.0019	0.0006	0.0080
$1s$-$2p$:	RM2D(15)	0.029	0.0005	0.050	0.046	0.103	0.0043	0.0022	0.025
	RM2D(20)	0.029	0.0005	0.050	0.046				
	FDPM	0.029	0.0005	0.049	0.045	0.103	0.0042	0.0022	0.025
$2s$-$2s$:	RM2D(15)	5.986	7.254	27.83	13.59	36.66	93.58	12.91	22.45
	RM2D(20)	5.988	7.281	27.81	13.58				
	FDPM	5.985	7.281	27.77	13.52	36.59	93.52	12.89	22.34
$2s$-$2p$:	RM2D(15)	3.638	0.00005	5.549	9.365	4.362	70.47	29.22	56.31
	RM2D(20)	3.638	0.00001	5.544	9.383				
	FDPM	3.637	0.00003	5.550	9.346	4.360	70.46	29.22	56.30
$2p$-$2p$:	RM2D(15)	3.242	17.01	10.68	96.30	41.16	64.18	27.20	133.4
	RM2D(20)	3.240	17.00	10.69	96.26				
	FDPM	3.243	17.00	10.72	96.32	41.19	64.22	27.18	133.3

TABLE VI. As for Table III, but at a collision energy of 0.81 Ry. The present results are compared with those of the finite-difference propagation method (FDPM) [19], the finite-element method (FEM) [18], the convergent close-coupling method (CCC) [31], and the intermediate-energy R-matrix method (IERM) [21].

	Method	^1S	^3S	$^1P^o$	$^3P^o$	^1D	^3D	$^1F^o$	$^3F^o$
$1s$-$1s$:	RM2D(15)	0.571	3.693	0.0015	1.991	0.064	0.134	0.011	0.034
	RM2D(20)	0.571	3.693	0.0015	1.991				
	FDPM	0.570	3.693	0.0016	2.019	0.064	0.134	0.011	0.035
	FEM	0.570	3.692	0.0017	2.005	0.063	0.131	0.012	0.036
	CCC	0.565	3.692	0.0016	1.986	0.064	0.132	0.011	0.034
	IERM	0.564	3.692	0.0015	1.989	0.063	0.130	0.011	0.033
$1s$-$2s$:	RM2D(15)	0.059	0.0012	0.0034	0.052	0.061	0.0028	0.0008	0.0098
	RM2D(20)	0.059	0.0012	0.0034	0.052				
	FDPM	0.059	0.0012	0.0034	0.052	0.061	0.0028	0.0008	0.0097
	FEM	0.063	0.0013	0.0048	0.055	0.056	0.0029	0.0009	0.0099
	CCC	0.057	0.0014	0.0033	0.054	0.058	0.0028	0.0010	0.0107
	IERM	0.059	0.0012	0.0034	0.052	0.063	0.0024	0.0010	0.0096
$1s$-$2p$:	RM2D(15)	0.026	0.0006	0.052	0.047	0.111	0.0059	0.0030	0.032
	RM2D(20)	0.026	0.0006	0.052	0.047				
	FDPM	0.026	0.0006	0.052	0.047	0.111	0.0058	0.0030	0.032
	FEM	0.023	0.0008	0.051	0.047	0.116	0.0051	0.0033	0.035
	CCC	0.025	0.0006	0.053	0.050	0.111	0.0069	0.0036	0.036
	IERM	0.026	0.0006	0.052	0.048	0.100	0.0058	0.0031	0.032
$2s$-$2s$:	RM2D(15)	7.022	10.39	20.26	7.535	29.47	95.12	11.40	22.75
	RM2D(20)	7.028	10.41	20.24	7.538				
	FDPM	7.022	10.41	20.23	7.575	29.43	95.12	11.39	22.67
	CCC	7.077	10.49	20.19	7.771	31.55	105.7	11.98	22.40
$2s$-$2p$:	RM2D(15)	2.980	0.422	3.393	13.24	2.476	54.52	24.61	40.78
	RM2D(20)	2.978	0.425	3.392	13.25				
	FDPM	2.979	0.423	3.393	13.20	2.477	54.51	24.61	40.77
	CCC	2.982	0.619	3.313	12.96	2.726	52.22	25.25	44.32
$2p$-$2p$:	RM2D(15)	1.959	12.61	10.82	73.81	35.82	50.25	21.75	116.2
	RM2D(20)	1.957	12.59	10.83	73.78				
	FDPM	1.960	12.59	10.84	73.83	35.84	50.28	21.74	116.2
	CCC	1.919	12.41	10.99	75.48	35.33	48.19	21.16	116.9

The computer package implementing the 2D R-matrix propagator consists of two programs. The first (PROPA) generates the one-electron basis in each sector, then constructs and diagonalizes the two-electron Hamiltonian matrix in each elementary domain. These tasks are independent of the collision energy. The second program (PROPB) performs the 2D propagation of the R matrix and the matching with asymptotic solutions to obtain the K matrix and cross sections at each collision energy. Since the 2D propagation method involves mainly matrix multiplications, inversions and diagonalizations, it has been efficiently implemented, using machine optimized libraries (BLAS, LAPACK, ESSL). For the calculations reported here, PROPA required approximately 15 min CPU time on a Cray C90 for the partial waves ^1S and ^3S, while PROPB took on average 7 s per energy to calculate phase shifts and cross sections for all possible transitions. For $L=2$, these times reached nearly 2 h for PROPA and approximately 80 s per energy for PROPB. On our local IBM RS6000 workstations, the time required is increased by a factor 6 or 7.

A. Elastic scattering below the $n=2$ threshold

In Table I we present phase shifts for $L=0$, 1, 2, and 3 at wave numbers $k=0.1$–0.8. We compare our results with those of the FEM [18], FDPM [19], and IERM [21] methods, and several variational calculations [32–35]. In general the agreement between all sets of results is excellent. We remark that for the ^1S partial wave, the IERM results are slightly smaller than those of the four other methods, but for ^3S and $^{3,1}P^o$, the phase shifts are essentially the same (to within 0.001). For $L=2$ and at low energy ($k=0.1$), the FEM results differ from those of the other methods, possibly indicating that the box used was not sufficiently large. For $L=3$, below $k=0.4$, the RM2D results tend to be slightly larger than the other results. At higher energies there is again excellent agreement between all methods.

The series of resonances converging to the $n=2$ threshold has been the subject of numerous studies. To a good approximation, in the vicinity of an isolated resonance the phase shift can be fitted to the form

$$\tan(\delta-\delta_0)=\frac{\Gamma}{2(E_R-E)}, \tag{3.1}$$

TABLE VII. As for Table III, but at a collision energy of 0.82 Ry.

	Method	^1S	^3S	$^1P^o$	$^3P^o$	^1D	^3D	$^1F^o$	$^3F^o$
$1s$-$1s$:	RM2D(15)	0.556	3.645	0.0018	1.966	0.065	0.135	0.011	0.034
	RM2D(20)	0.556	3.645	0.0018	1.966				
	FDPM	0.555	3.645	0.0019	1.976	0.065	0.134	0.011	0.035
$1s$-$2s$:	RM2D(15)	0.061	0.0013	0.0038	0.054	0.064	0.0036	0.0011	0.011
	RM2D(20)	0.062	0.0013	0.0038	0.054				
	FDPM	0.062	0.0013	0.0038	0.054	0.063	0.0036	0.0010	0.011
$1s$-$2p$:	RM2D(15)	0.024	0.0007	0.055	0.048	0.120	0.0074	0.0038	0.037
	RM2D(20)	0.024	0.0007	0.055	0.048				
	FDPM	0.024	0.0007	0.054	0.048	0.120	0.0074	0.0037	0.037
$2s$-$2s$:	RM2D(15)	7.750	12.28	14.81	5.814	24.60	94.32	10.35	24.19
	RM2D(20)	7.755	12.30	14.80	5.820				
	FDPM	7.750	12.30	14.78	5.797	24.53	94.21	10.35	24.10
$2s$-$2p$:	RM2D(15)	2.029	1.163	2.378	16.06	1.534	42.42	21.31	30.46
	RM2D(20)	2.027	1.164	2.379	16.07				
	FDPM	2.028	1.163	2.379	16.05	1.533	42.43	21.31	30.47
$2p$-$2p$:	RM2D(15)	1.311	9.266	10.64	56.84	31.32	41.95	17.95	102.5
	RM2D(20)	1.309	9.253	10.65	56.82				
	FDPM	1.312	9.252	10.66	56.83	31.34	42.01	17.93	102.4

where E_R is the resonance energy (position), Γ is the width and δ_0 is the background value of the phase shift, assumed constant near the resonance. Using a least-squares fitting procedure on our data, we have calculated positions and widths for the first resonances in the partial waves ^1S, $^3P^o$, and ^1D. These are compared in Table II with the positions and widths obtained by other calculations, as well as some experimental measurements. For ^1S, all theories agree well for both the position and the width. For $^3P^o$, the hyperspherical coordinate method finds the resonance at a slightly higher energy than the other methods, with a larger width. For ^1D, the various theories agree reasonably well over the position of the resonance, but there is less agreement over the width: in particular, the theoretical predictions are significantly larger than the measured value.

B. Scattering between the $n=2$ and 3 thresholds

The results presented in the preceding section concern single channel elastic scattering, and establish the accuracy of the RM2D propagator for describing such a process. For scattering energies between the $n=2$ and 3 thresholds, excitation processes become possible, providing a more stringent test of theory, in particular since they involve a long-range dipole coupling between degenerate s and p states. In Tables III–VIII, we present partial cross sections for $L=0$–3 and

TABLE VIII. As for Table III, but at a collision energy of 0.85 Ry.

	Method	^1S	^3S	$^1P^o$	$^3P^o$	^1D	^3D	$^1F^o$	$^3F^o$
$1s$-$1s$:	RM2D(15)	0.519	3.507	0.0028	1.889	0.066	0.138	0.012	0.035
	RM2D(20)	0.519	3.507	0.0028	1.889				
	FDPM	0.518	3.508	0.0029	1.898	0.065	0.137	0.012	0.036
$1s$-$2s$:	RM2D(15)	0.055	0.0017	0.0060	0.055	0.074	0.0059	0.0021	0.011
	RM2D(20)	0.055	0.0017	0.0060	0.055				
	FDPM	0.055	0.0017	0.0060	0.055	0.074	0.0059	0.0021	0.012
$1s$-$2p$:	RM2D(15)	0.025	0.0010	0.067	0.046	0.152	0.011	0.0069	0.048
	RM2D(20)	0.025	0.0010	0.067	0.046				
	FDPM	0.025	0.0010	0.067	0.046	0.152	0.011	0.0069	0.048
$2s$-$2s$:	RM2D(15)	7.033	13.27	6.042	7.793	18.13	83.66	8.532	27.43
	RM2D(20)	7.035	13.29	6.045	7.805				
	FDPM	7.032	13.28	6.033	7.791	18.09	83.58	8.524	27.33
$2s$-$2p$:	RM2D(15)	0.687	2.792	2.052	17.69	0.491	21.44	15.32	14.84
	RM2D(20)	0.684	2.782	2.050	17.70				
	FDPM	0.686	2.785	2.049	17.69	0.490	21.45	15.31	14.84
$2p$-$2p$:	RM2D(15)	0.598	3.690	8.846	28.00	21.54	30.66	11.47	73.40
	RM2D(20)	0.599	3.687	8.850	27.99				
	FDPM	0.599	3.685	8.860	27.99	21.54	30.71	11.47	73.38

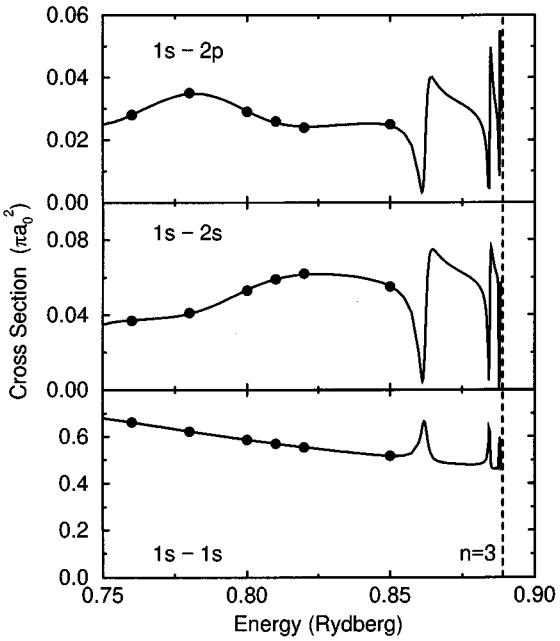

FIG. 2. ^1S partial cross sections (in units of πa_0^2) for the $1s$-$1s$, $1s$-$2s$, $1s$-$2p$ transitions between the $n=2$ and 3 thresholds. Solid line, RM2D(15) results; ●, FDPM results [19].

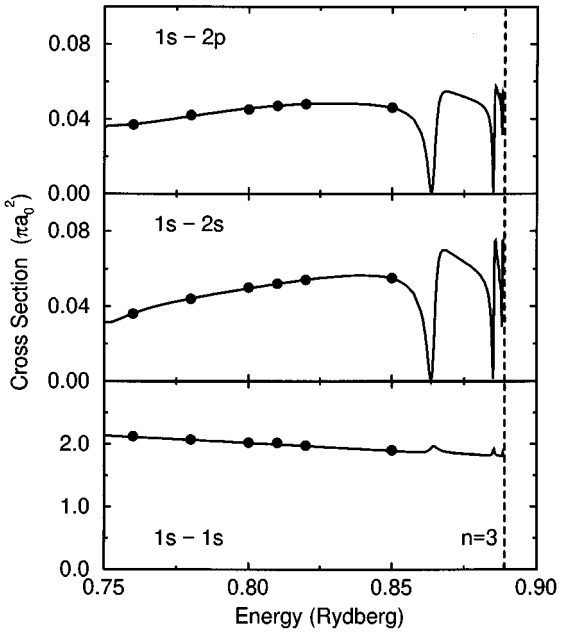

FIG. 3. $^3P^o$ partial cross sections (in units of πa_0^2) for the $1s$-$1s$, $1s$-$2s$, $1s$-$2p$ transitions between the $n=2$ and 3 thresholds. Solid line, RM2D(15) results; ●, FDPM results [19].

both singlet and triplet symmetries, for all possible elastic and excitation processes involving the $1s$, $2s$, and $2p$ states, at energies 0.76, 0.78, 0.80, 0.81, 0.82, and 0.85 Ry. We compare our results with those of the FDPM [19] at all these energies, and with those of other methods at 0.81 Ry.

The partial cross sections presented in Table III correspond to a total energy 0.76 Ry, very close to the $n=2$ threshold, so that the energies in channels involving the $2s$ and $2p$ states are very small (0.01 Ry). This gives rise to very large cross sections for transitions between these states. In addition, there is a narrow shape resonance in the $^1P^o$ partial wave at 0.752 Ry. For partial waves $L=0$, 1, 2 our results are in excellent agreement (to within 1%) with those of the FDPM [19], apart from the $1s$-$2s$ ^3D cross section, which is very small. For $L=3$, the discrepancy can reach 10%, but again this is for a very small cross section. A similar pattern can be seen for the other energies considered (Tables IV–VIII).

In Table VI we compare our partial cross sections at 0.81 Ry with those from three additional methods: FEM [18], IERM [21], and CCC [31]. The CCC calculation used a basis of ten s, nine p, eight d, and seven f functions, allowing accurate representations of the hydrogenic wave functions for $n \leqslant 3$. All possible angular couplings involving these target states were included, so that for $L=2$, 3 there are more couplings in the CCC calculation than in the RM2D and FDPM calculations. We note that the current CCC results correct those presented in [19], which suffered from some numerical difficulties.

The agreement between all sets of results is generally very good (to within 1% or 2%), except for certain isolated cases. There is always excellent agreement between the RM2D and FDPM results. Differences between our results and those of the CCC calculation for $L=2$,3 may be partially explained by differences in the angular couplings used. The CCC $2s$-$2p$ ^3S cross section, however, differs by 30% although the angular couplings are the same. This suggests that there may be some convergence difficulties for the CCC calculation in this energy range [31]. Another large difference (40%) can be observed for the $1s$-$2s$ $^1P^o$ FEM result. For the $1s$-$1s$ transition, the IERM results tend to agree more with those of the CCC calculation than those of the RM2D

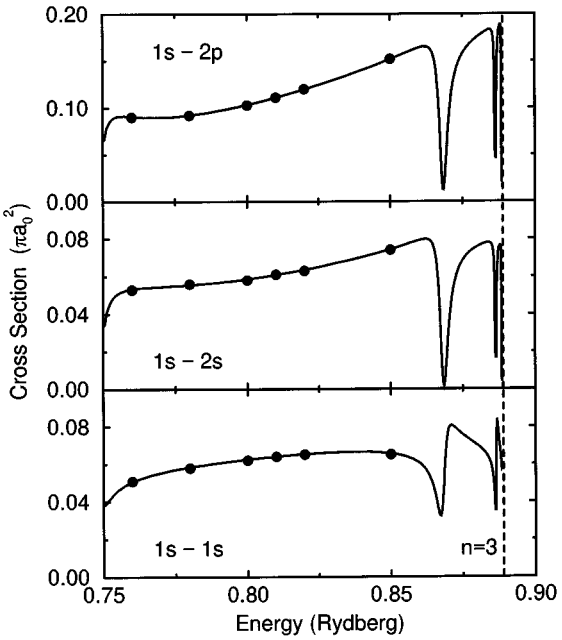

FIG. 4. ^1D partial cross sections (in units of πa_0^2) for the $1s$-$1s$, $1s$-$2s$, $1s$-$2p$ transitions between the $n=2$ and 3 thresholds. Solid line, RM2D(15) results; ●, FDPM results [19].

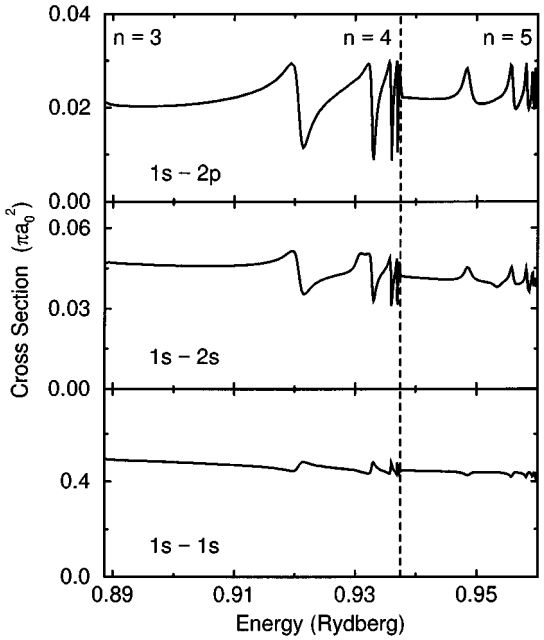

FIG. 5. ^1S partial cross sections (in units of πa_0^2) for the $1s$-$1s$, $1s$-$2s$, $1s$-$2p$ transitions between the $n=3$ and 5 thresholds.

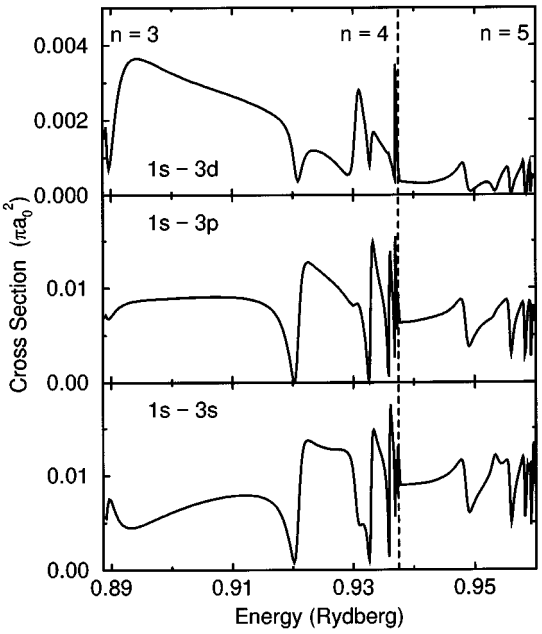

FIG. 6. ^1S partial cross sections (in units of πa_0^2) for the $1s$-$3s$, $1s$-$3p$, $1s$-$3d$ transitions between the $n=3$ and 5 thresholds.

calculation, but for the $1s$-$2s$ and $1s$-$2p$ transitions the situation is reversed.

In Figs. 2–4, we compare our results between the $n=2$ and 3 thresholds for ^1S, $^3P^o$, and ^1D, together with the FDPM results of Wang and Callaway [19]. These demonstrate the efficiency of our method at energies close to threshold, where a fine energy mesh is required in order to resolve detailed resonance structure. At such energies, the asymptotic solutions are more slowly convergent and it is necessary to propagate the R matrix quite far (typically a few hundred a.u.) before the matching can be performed.

C. Scattering between the $n=3$ and 5 thresholds

The calculation presented in the preceeding section serves as a first stringent test of the RM2D method. In order to make a detailed comparison with other results, in particular the FDPM, we restricted our calculation by using parameters as close as possible to those used in [19]. For example, we used the same angular couplings and propagated out to only 60 a.u. While this distance is sufficient to obtain converged cross sections for excitation into the $n=2$ states, it is not adequate if we wish to study excitation into higher states, which is our goal.

As an illustration of the power of the new method, we present in Figs. 5 and 6 some preliminary results for ^1S elastic scattering and excitation into the $n=2$ and 3 levels, between the $n=3$ and 5 thresholds. By propagating out to $r_{\rm out}=100$ a.u., we have a very precise representation of all states with $n\leqslant 5$, while the energies of the $n=6$ states are correct to within 0.2%. In order to obtain converged cross sections at energies close to threshold, the 1D Light-Walker propagator is used out to several hundred a.u. We have performed two calculations, with orbital angular momenta $l\leqslant 4$ and $l\leqslant 5$, respectively. The results are practically identical over the energy range considered, indicating that convergence has already been achieved with $l\leqslant 4$.

The figures clearly show the series of resonances converging to the $n=4$ and 5 thresholds. These series have been studied in detail using, for example, pseudostate expansions [6], hyperspherical coordinates [36], complex coordinate rotation methods [40], and an R-matrix method [41]. The positions of the lowest resonances in our results appear to be in good agreement with those of other calculations, and we are currently performing a systematic fitting of the resonances in order to make a more quantitative comparison.

IV. CONCLUSIONS

The two-dimensional R matrix propagator was first established as an accurate and efficient method for studying electron-hydrogen collisions in the s-wave model [16]. In the current work, we have extended the method to arbitrary orbital angular momenta and applied it to the study of elastic scattering and excitation up to the $n=3$ threshold. We have obtained phase shifts, resonance parameters, and partial cross sections in very good agreement with those of other accurate methods. We have also shown the efficiency of our method above the $n=3$ threshold, confirming its potential for studying excitation into highly excited states.

A detailed study of resonances is currently underway, and we are also extending the calculations to higher partial waves in order to obtain converged cross sections which can be compared with experimental data.

ACKNOWLEDGMENTS

We thank Igor Bray for providing unpublished results from a convergent close-coupling calculation. This work was

supported in part by the European Community, Contracts No. ERB CHBI CT920082, No. ERB CHRX CT920013, and No. ERB CHRX CT930350 (Human Capital and Mobility Programme). All computation was performed on local IBM RS6000 workstations and on the Cray C98 at the Institut du Développement et des Ressources en Informatique Scientifique (IDRIS), Orsay, France with time allocated under Projects No. 940369 and No. 950369.

[1] L. Castillejo, I. C. Percival, and M. J. Seaton, Proc. R. Soc. London, Ser. A **254**, 259 (1960).
[2] I. E. McCarthy and B. Shang, Phys. Rev. A **46**, 3958 (1992).
[3] M. Gailitis and R. Damburg, Proc. Phys. Soc. London **82**, 192 (1963).
[4] S. Trajmar and I. Kanik, in *Atomic and Molecular Processes in Fusion Edge Plasmas*, edited by R. K. Janev (Plenum, New York, 1995), Chap. 3.
[5] I. C. Percival and M. J. Seaton, Proc. Cambridge Philos. Soc. **53**, 654 (1957).
[6] J. Callaway, Phys. Rev. A **26**, 199 (1982).
[7] D. H. Oza and J. Callaway, Phys. Rev. A **27**, 2840 (1983).
[8] P. G. Burke and W. B. Eissner, in *Atoms in Astrophysics*, edited by P. G. Burke, W. B. Eissner, D. G. Hummer, and I. C. Percival (Plenum, New York, 1983), Chap. 1.
[9] K. Bartschat, Phys. Rep. **180**, 1 (1989).
[10] J. Callaway and K. Unnikrishnan, Phys. Rev. A **48**, 4292 (1993).
[11] I. Bray and A. T. Stelbovics, Phys. Rev. A **46**, 6995 (1992).
[12] S. Watanabe, Y. Hosoda, and D. Kato, J. Phys. B **26**, L495 (1993).
[13] A. Temkin, Phys. Rev. **126**, 130 (1962).
[14] R. Poet, J. Phys. B **13**, 2995 (1980); **14**, 91 (1981).
[15] J. Callaway and D. H. Oza, Phys. Rev. A **29**, 2416 (1984).
[16] M. Le Dourneuf, J.-M. Launay, and P. G. Burke, J. Phys. B **23**, L559 (1990).
[17] I. Bray and A. T. Stelbovics, Phys. Rev. Lett. **69**, 52 (1992).
[18] J. Shertzer and J. Botero, Phys. Rev. A **49**, 3573 (1994).
[19] Y. D. Wang and J. Callaway, Phys. Rev. A **50**, 2327 (1994).
[20] P. G. Burke, C. J. Noble, and M. P. Scott, Proc. R. Soc. London **410**, 289 (1987).
[21] T. Scholz, M. P. Scott, and P. G. Burke, J. Phys. B **21**, L139 (1988).
[22] B. R. Odgers, M. P. Scott, and P. G. Burke, J. Phys. B **28**, 2973 (1995).
[23] C. Bloch, Nucl. Phys. **4**, 503 (1957).
[24] A. R. Edmonds, *Angular Momentum in Quantum Mechanics* (Princeton University Press, Princeton, NJ, 1957).
[25] P. J. A. Buttle, Phys. Rev. **160**, 719 (1967).
[26] I. Shimamura, J. Phys. B **10**, 2597 (1977).
[27] V. M. Burke and C. J. Noble, Comput. Phys. Commun. **85**, 471 (1995).
[28] J. C. Light and R. B. Walker, J. Chem. Phys. **65**, 4272 (1976).
[29] P. G. Burke and H. M. Schey, Phys. Rev. **126**, 147 (1962).
[30] M. Gailitis, J. Phys. B **9**, 843 (1976).
[31] I. Bray (private communication).
[32] I. Shimamura, J. Phys. Soc. Jpn. **30**, 1702 (1971).
[33] J. N. Das and M. R. H. Rudge, J. Phys. B **9**, L131 (1976).
[34] D. Register and R. T. Poe, Phys. Lett. **51A**, 431 (1975).
[35] J. Callaway, Phys. Lett. **65A**, 199 (1978).
[36] H. Sadeghpour, J. Phys. B **25**, L29 (1992).
[37] L. Sanche and P. D. Burrow, Phys. Rev. Lett. **29**, 1139 (1972).
[38] J. Williams, *Electron and Photon Interactions with Atoms* (Plenum, New York, 1976).
[39] C. D. Warner, G. C. King, P. Hammond, and J. Slevin, J. Phys. B **19**, 3297 (1986).
[40] Y. K. Ho and J. Callaway, Phys. Rev. A **27**, 1887 (1983); **34**, 130 (1986).
[41] A. Pathak, A. E. Kingston, and K. A. Berrington, J. Phys. B **21**, 2939 (1988); A. Pathak, P. G. Burke, and K. A. Berrington, *ibid.* **22**, 2759 (1989).